AFRL-AFOSR-VA-TR-2020-0144

# Rational Design of Composite Solid Electrolyte for Structural Energy Storage

Yuan Yang
THE TRUSTEES OF COLUMBIA UNIVERSITY IN THE CITY OF NEW YORK

07/29/2020
Final Report

Air Force Research Laboratory
AF Office Of Scientific Research (AFOSR)/ RTA1
Arlington, Virginia 22203
Air Force Materiel Command

# REPORT DOCUMENTATION PAGE

*Form Approved*
*OMB No. 0704-0188*

| | | |
|---|---|---|
| **1. REPORT DATE** *(DD-MM-YYYY)*<br>20-08-2020 | **2. REPORT TYPE**<br>Final Performance | **3. DATES COVERED** *(From - To)*<br>01 Aug 2018 to 31 Jul 2020 |

**4. TITLE AND SUBTITLE**
Rational Design of Composite Solid Electrolyte for Structural Energy Storage

**5a. CONTRACT NUMBER**

**5b. GRANT NUMBER**
FA9550-18-1-0410

**5c. PROGRAM ELEMENT NUMBER**
61102F

**6. AUTHOR(S)**
Yuan Yang

**5d. PROJECT NUMBER**

**5e. TASK NUMBER**

**5f. WORK UNIT NUMBER**

**7. PERFORMING ORGANIZATION NAME(S) AND ADDRESS(ES)**
THE TRUSTEES OF COLUMBIA UNIVERSITY IN THE CITY OF NEW YORK
116TH AND BDWY
NEW YORK, NY 10027 US

**8. PERFORMING ORGANIZATION REPORT NUMBER**

**9. SPONSORING/MONITORING AGENCY NAME(S) AND ADDRESS(ES)**
AF Office of Scientific Research
875 N. Randolph St. Room 3112
Arlington, VA 22203

**10. SPONSOR/MONITOR'S ACRONYM(S)**
AFRL/AFOSR RTA1

**11. SPONSOR/MONITOR'S REPORT NUMBER(S)**
AFRL-AFOSR-VA-TR-2020-0144

**12. DISTRIBUTION/AVAILABILITY STATEMENT**
A DISTRIBUTION UNLIMITED: PB Public Release

**13. SUPPLEMENTARY NOTES**

**14. ABSTRACT**

This project focuses on developing structural batteries with high energy density. In the last two years, we have developed two systems for structural energy storage. The first one is to combine high-energy-density Li/S battery with T300 carbon fibers and ceramic/polymer composite solid electrolyte, which leads to high modulus of 10-15 GPa at cell level and high strength of ~150 MPa. The second one is solid state Li batteries with a solid polymer/ceramic electrolyte inspired by the brick-mortar structure of nacre, where polymer filler enhances the fracture energy of the ceramic electrolyte so that the electrolyte is much tougher than pure ceramic electrolyte.

The major achievements include: 1) Solid composite electrolytes with high ionic conductivities and good mechanical properties, such as a nacre-like LATP/polymer electrolyte with conductivity of~ 8 x 1011-4 Siem, and fracture strain, flexural strength and modulus of 1.1 %, 35 MPa and 7.8 GPa, respectively, and a BN/PVdF composite electrolyte with conductivity of~ 3.6 x 1011-4 Siem, which functions well under compression of 190 MPa (limit of current instrument, 2) prototype Li-S battery demonstrated with structural components (e.g. carbon fabric-reinforced cathode/anode). The capacity reaches 1100 mAh/g with a retention of 95%/100 cycles. The cell functions well under a compressive pressure of 20 MPa, while conventional cells fail at ~10 MPa, and 3) one paper entitled 'Nacre-Inspired Composite Electrolytes for Load-Bearing Solid-State Lithium Metal Batteries' published in Advanced Materials (IF: 25.8), which has been cited for 9 times in only eight months, and one paper entitled 'Mechanically-robust structural lithium-sulfur battery with high energy density' under review in Energy Storage Materials (IF: 16.0)

**15. SUBJECT TERMS**
Composite Solid Electrolyte

Standard Form 298 (Rev. 8/98)
Prescribed by ANSI Std. Z39.18

| | | | | | |
|---|---|---|---|---|---|
| **16. SECURITY CLASSIFICATION OF:** | | | **17. LIMITATION OF ABSTRACT** | **18. NUMBER OF PAGES** | **19a. NAME OF RESPONSIBLE PERSON**<br>BIRKAN, MITAT |
| **a. REPORT** | **b. ABSTRACT** | **c. THIS PAGE** | | | |
| Unclassified | Unclassified | Unclassified | UU | | **19b. TELEPHONE NUMBER** *(Include area code)*<br>703-696-7234 |

Standard Form 298 (Rev. 8/98)
Prescribed by ANSI Std. Z39.18

DISTRIBUTION A: Distribution approved for public release

# Rational Design of Composite Solid Electrolyte for Structural Energy Storage

Grant No.: FA9550-18-1-0410

PI: Yuan Yang (Columbia University) Project Period: 07/01/2018 – 06/31/2020

## Project Goals

- Solid Electrolyte with conductivity > $5 \times 10^{-4}$ S/cm, and compressive strength of 250 MPa.
- Demonstration of structural Li-S batteries with composite electrolyte above.

## Summary of Major Achievement

This project focuses on developing structural batteries with high energy density. In the last two years, we have developed two systems for structural energy storage (Fig. 1). The first one is to combine high-energy-density Li/S battery with T300 carbon fibers and ceramic/polymer composite solid electrolyte, which leads to high modulus of 10-15 GPa at cell level and high strength of ~150 MPa (Fig. 1a-d). The second one is solid state Li batteries with a solid polymer/ceramic electrolyte inspired by the brick-mortar structure of nacre, where polymer filler enhances the fracture energy of the ceramic electrolyte so that the electrolyte is much tougher than pure ceramic electrolyte (Fig. 1e-h). The major achievements are.

- Solid composite electrolytes with high ionic conductivities ($\sigma$) and good mechanical properties.
  - A nacre-like LATP/polymer electrolyte with $\sigma$ of ~ $8 \times 10^{-4}$ S/cm, and fracture strain, flexural strength and modulus of 1.1%, 35 MPa and 7.8 GPa, respectively.
  - A BN/PVdF composite electrolyte with $\sigma$ of ~ $3.6 \times 10^{-4}$ S/cm, which functions well under compression of 190 MPa (limit of current instrument)
- Prototype Li-S battery demonstrated with structural components (e.g. carbon fabric-reinforced cathode/anode). The capacity reaches 1100 mAh/g with a retention of 95%/100 cycles (Fig. 1d). The cell functions well under a compressive pressure of 20 MPa, while conventional cells fail at ~10 MPa.
- One paper entitled "Nacre-Inspired Composite Electrolytes for Load-Bearing Solid-State Lithium Metal Batteries" published in *Advanced Materials* (IF: 25.8), which has been cited for 9 times in only eight months, and one paper entitled " Mechanically-robust structural lithium-sulfur battery with high energy density" under review in *Energy Storage Materials* (IF: 16.0)

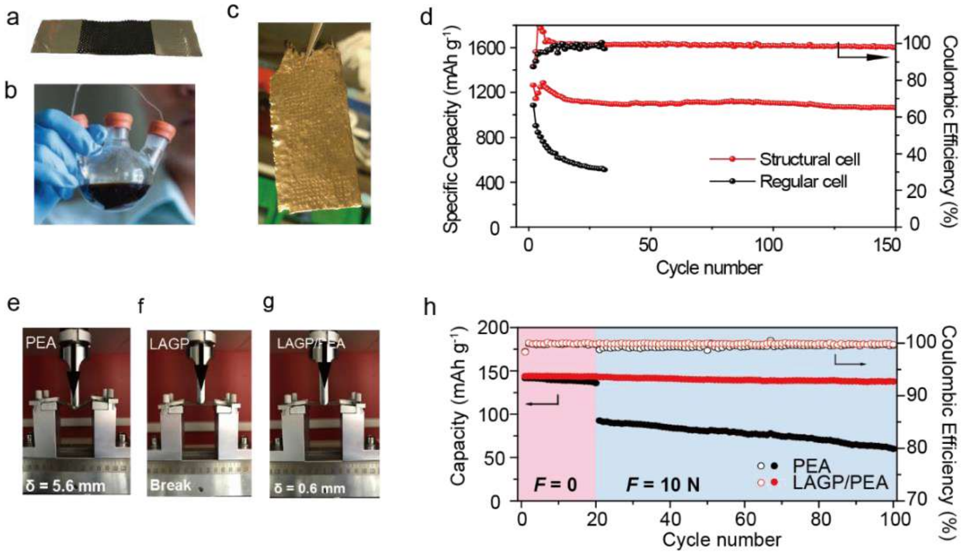

**Figure 1.** (a-c) (a) Carbon fiber, (b) lithium polysulfide solution and (c) Li/C fiber composite anode used in structural battery. (d) Cycling performance of a structural Li-S battery vs. a conventional Li-S battery based on carbon black/sulfur particle electrode and pure lithium metal anode. (e-g) A $LiFePO_4$/Li cell with nacre-like solid electrolyte under flexing. (h) Comparison of a $LiFePO_4$/Li cell with nacre-like solid electrolyte (red) and polymer solid electrolyte (black).

## Progress Details

### 1. Structural Li-S batteries with high energy density.

1.1 Introduction.

Lightweighting is critical for enhancing the energy efficiency of transportation, such as aircrafts and electrical vehicles[1, 2]. The development of multifunctional materials to integrate different functions into a single component is an attractive concept in lightweighting[3, 4]. For example, structural components can be used for energy production (e.g. solar cells or kinetic energy harvesting)[5, 6] or storage (e.g. supercapacitors or batteries)[7-9] to reduce the overall weight. To combine energy storage and structural functions together, the structural battery must have both robust mechanical properties to adapt to various kinds of deformation, such as tensile or compressive stress, and excellent electrochemical performance, such as high energy density and long cycle life. Moreover, these batteries should function safely under mechanical deformation that could be encountered during operation.

In recent years, several groups have conducted pioneering works on structural supercapacitors by using carbon fiber or graphene-based materials as the mechanical support and even active materials[10-14]. Reasonable electrochemical performance with improved mechanical properties has been demonstrated, but the specific energy is typically lower than 1.0 Wh $kg^{-1}$[15, 16]. The same strategy has been applied to structural batteries but limited success has been achieved.[12, 15] The main reason lies in the lack of structural materials that can endure environmental stress as well as maintain synergistic lifespan in battery system. On one hand, the repeated volume change of electrode materials in batteries makes them easy to delaminate from planar current collectors (Fig. 2a) or carbon fibers (Fig. 2b), which not only increases the electronic resistance but also reduces mechanical strength of the whole battery[15, 17, 18]. If ions intercalate into carbon fibers (e.g. in Li-ion battery anodes), the mechanical strength of carbon fibers will be significantly compromised.[19, 20] For another, conventional battery separators are flammable and do not have enough mechanical strength, especially in the weak direction.

To address these issues, we propose an electrodeposition-like strategy for electrodes and develop a nanocomposite separator with enhanced mechanical and thermal properties. For electrodes, active materials are coated onto mechanically robust carbon fabric (CF), thereby minimizing the risk of delamination of electrode materials from the CF matrix. For separator, high-modulus BN nanoplatelets are introduced to improve the mechanical modulus of separator, even under mechanical deformation. To demonstrate this concept, we use Li-S battery as an example in this report; however, this configuration is also applicable for other systems, such as Li-$I_2$, Zn-$Br_2$, and Li-$O_2$ batteries. Specifically, T300 CF is combined with 1 M polysulfide catholyte as the cathode, enabling sulfur and $Li_2S_2$/$Li_2S$ to be electrodeposited onto the CF conformally during the charge/discharge process, and thus avoiding poor contact between conventional electrode particles (e.g. $LiCoO_2$ particles) and carbon fibers (Fig. 2b). At the anode side, molten lithium is infiltrated into the carbon fiber matrix. Although Li intercalation reduces the mechanical properties of carbon fibers, the excessive lithium metal can act as a glue to bind lithiated carbon fibers together, thereby enhancing the mechanical strength of the anode.

The reinforced cathode and anode have Young's modulus of 9.2 ± 1.2 GPa and 4.5 ± 0.6 GPa, respectively, and corresponding ultimate tensile strength (UTS) of 214 ± 16 MPa and 53 ± 7 MPa, which are all 1-2 orders of magnitude higher than those of conventional particle-based electrodes. In addition to improving the mechanical properties of electrodes, we also developed a thermally stable BN/PVdF composite separator to enhance the compressive strength of the prepared cells. Owing to the introduction of BN nanosheets, the as-fabricated BN/PVdF composite separator possesses UTS of 13.1 ± 1.2 MPa and isotropic Young's modulus of 1.2 ± 0.2 GPa, significantly superior to that of the regular PE separator (Celgard 2325) in its transverse direction (8.0 ± 0.6 MPa and 0.26 ± 0.05 GPa, respectively). Combining the well-designed structural electrodes with the BN/PVdF separator, the structural Li-S battery shows excellent electrochemical performance, delivering an initial discharge capacity of 1266 mAh $g^{-1}$ and capacity retention of 81% after 200 cycles at 0.2 C. These results demonstrate the feasibility of this new strategy to improve the mechanical strength of structural batteres with high energy density.

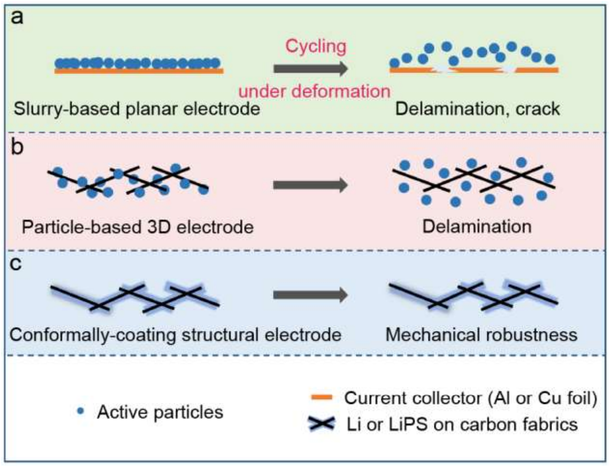

**Figure 2.** The design principle of electrodeposition-like electrodes for structural energy storage. (a) An illustration of the intrinsically low mechanical strength of particle-based planar electrodes, sufferring from the delamination of active materials or crack of current collector (Al or Cu foil) during cycling under deformation. (b) An illustration of the delamination of active materials from carbon fibers during cycling under deformation, due to weak interactions between these two parts. (c) An illustration of the enhanced strength via electrodeposition-like reaction on structural skeleton (e.g. the electrochemical conversion of lithium polysulfides to suflur conformally on carbon fabrics).

## 1.2 Results and discussion

In our design, the cathode is made of commercial T300 CF in combination with 2.0 M $Li_2S_8$ (the concentration is based on [S]) in 1,3-dioxolane/1,2-dimethoxyethane (DOL/DME) as the structural skeleton. The pristine CF consists of horizontal and vertical carbon bundles where the diameter of filament is ~7 μm, which possesses UTS of 232 ± 8 MPa and Young's modulus of 22 ± 1.6 GPa based on three samples (Fig. 3c and 3d). However, since the polymer-based sizing agent on fiber surface impedes electron transport, the initial discharge capacity of the cathode is only ~ 300 mAh $g^{-1}$, as illustrated by the black curve in Fig. 3e. Upon cycling, the discharge capacity gradually increases to ~ 800 mAh $g^{-1}$ after 70 cycles, which might arise from the swelling and even dissolution of sizing agent in the electrolyte. This capacity, however, is relatively lower than previous reports.[21, 22]

To enhance the electrochemical performance, the pristine CF is heated in air remove the sizing agent. The OCF 500 ºC 2h, namely the sample that was heated at 500°C for 2 h is the optimal condition based on the balance of the electrochemical performance and the mechanical strength. The detailed mechanism of heating treatment-dependent electrochemical performance is further analyzed in supporting information, which in related to the intensity of C-C/C=O groups on CF surface. These heated samples are denoted as oxidized carbon fabric (OCF). Although OCF shows slightly compromised mechanical strength, such as UTS of 218 ± 14 MPa after heating, 214 ± 16 MPa after soaking in the polysulfide catholyte and 198 ± 17 MPa after electrodepositing $Li_2S$, however, such mechanical properties are still four times higher than conventional particle-based cathodes on Al foil (56 ± 5 MPa). The Young's modulus shows the same trend, which are 19 ± 1.7 GPa after heating, 9.2 ± 1.2 after soaking in 1 M polysulfide catholyte and 8.8 ± 2.1 GPa after electrodepositing $Li_2S$, much higher than sulfur particle-coated Al foil (6.4 ± 0.1 GPa). Despite this, the electrochemical performance dramatically improves after thermal treatment. The initial capacity reaches 1159 mAh $g^{-1}$ and the capacity retention is 91.9% after 150 cycles at 0.2 C (Fig. 3e). The excellent reversibility can be attributed to uniform deposition and improved interactions of polysulfide species onto the carbon fibers with large surface area. The properties of CF treated at temperatures and time are also studied, and 500 °C for 2 h discussed above is the optimal condition to balance the mechanical and electrochemical properties.

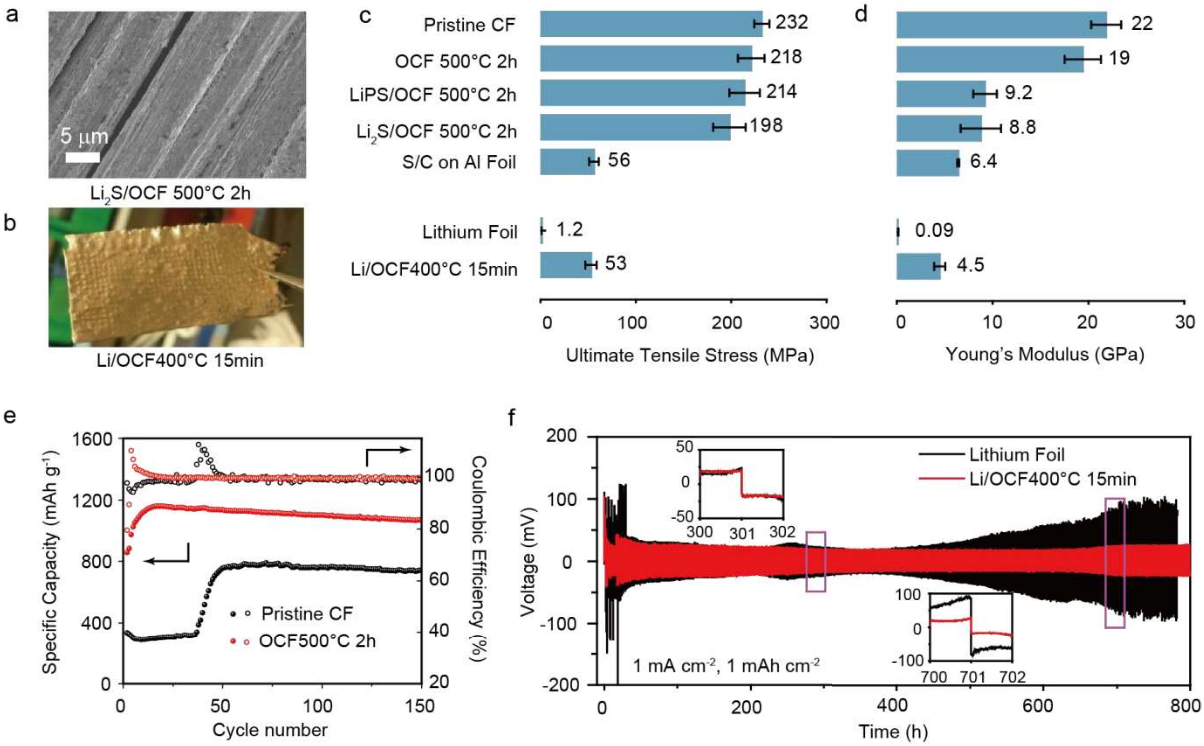

**Figure 3.** (a) The surface morphology of OCF after depositing $Li_2S$. (b) A digital image of a piece of OCF after infiltrating molten lithium metal inside. (c) The UTS and (d) Young's modulus of carbon fiber-reinforced electrodes in comparison to conventional particle-based electrodes. (e) The cycling performance of the polysulfide cathode with pristine CF (black curve) and OCF 500 °C 2 h (red curve). (f) The cycling stability of Li/Li symmetric cells with conventional Li foil (black) and Li/OCF composite in (b). The current and the deposited capacity are 1.0 mA $cm^{-2}$ and 1.0 mAh $cm^{-2}$, respectively. The inset shows the voltage profile at the 150th and 350th cycle.

On the other hand, lithium metal is infiltrated into OCF to enhance the mechanical strength of anode. It should be noted that the sizing agent on CF is first removed by heating at 400 °C in air for 15 min. Otherwise the CF shows lithiophobic behavior. Once thermally annealed, oxygen rich functional groups on carbon surface enable lithium metal to readily infiltrate inside[23, 24], and the OCF skeleton remarkably strengthens the lithium anode. Basically, the UTS improves from 1.2 ± 0.2 MPa (pure lithium foil) to 53 ± 7 MPa (CF/Li 400 °C15 min) while the Young's modulus increases dramatically from 0.09 ± 0.05 GPa to 4.5 ± 0.6 GPa, respectively (Fig. 3c and 3d). The significant enhancement originates from the load transfer from lithium metal to the interconnected OCF network, similar to the results in a previous report.[25]

The OCF-reinforced lithium anode with a thickness of ~ 250 um also shows improved electrochemical performance. As shown in Fig. 3f, the Li/Li symmetric cell with lithium/OCF electrodes exhibits a stable voltage profile during cycling and an overpotential as small as 20 mV over 800 h at a current density of 1.0 mA cm$^{-2}$ with an ether-based electrolyte (1.0 M LiTFSI with 2.0 wt% $LiNO_3$ in DOL/DME). In comparison, the cell using lithium foil electrodes shows poor cycling stability with increasing overpotential during repeated stripping/plating process. The improved performance might originate from larger surface area in the Li/OCF composite electrode.[24] Although Li fills most regions inside carbon fibers, there are always voids left that accommodates for the deposited lithium metal. Therefore, even at a higher current density of 3.0 mA cm$^{-2}$, the stability of lithium stripping/plating with Li/CF electrodes is much better than that in pure lithium anode.

In addition to introducing the OCF matrix to enhance the tensile strength/Young's modulus of electrode materials, we also develop a BN/PVdF composite to replace the conventional PE separator. As a solid matrix material, BN possesses several desirable attributes including electronic insulation, chemical inertness, thermal stability and mechanical robustness[26]. In view of this, a BN/PVdF composite separator was prepared by sonicating the crumpled-paper-like BN aggregates in a mixed IPA/DMF solvent, followed by connecting the BN nanosheets with flexible PVdF chains (Fig. 4a). Since BN is nonflammable and PVdF has a flash point over 400 °C[27, 28], the composite film is much more thermally stable than PE separator when ignited, even with the presence of electrolyte. When ignited by a lighter, the BN/PVdF separator is difficult to catch fire. Conversely, the PE seperator burns immediately (Fig. 4b). Mechanically, the BN/PVdF film shows higher UTS and modulus (13.1 ± 1.2 MPa and 1.2 ± 0.2 GPa respectively), which are much higher than those of PE separator at the weak transverse direction (8.0 ± 0.6 MPa and 0.26 ± 0.05 GPa) (Fig. 4c and 4d). In addition to standard mechanical measurements, we also explored how compression affects the ionic conductivity in the two kinds of separators, which helps evaluate how batteries behave under external impact. As shown in Fig. 4e, the BN/PVdF separator shows higher resistance at intermediate pressure. Regardless, the BN/PVdF separator outperforms the PE separator with relatively more stable conductivity when the compression exceeds 150 MPa. This result can be attributed to the high-modulus BN filler that maintains the integrity of the BN/PVdF separator at extremely high compressive stress. Since the resistivity increases only by a factor of 3 up to 180 MPa, it is still acceptable for electrochemical cycling. As shown in Fig. 4f, the Li/Li symmetrical cell with BN/PVdF separator wetted by liquid electrolyte delivers a stable voltage profile over 500 h at 1.0 mAh cm$^{-2}$ and 1.0 mA cm$^{-2}$, demonstrating excellent lithium plating/stripping reversibility.[29]

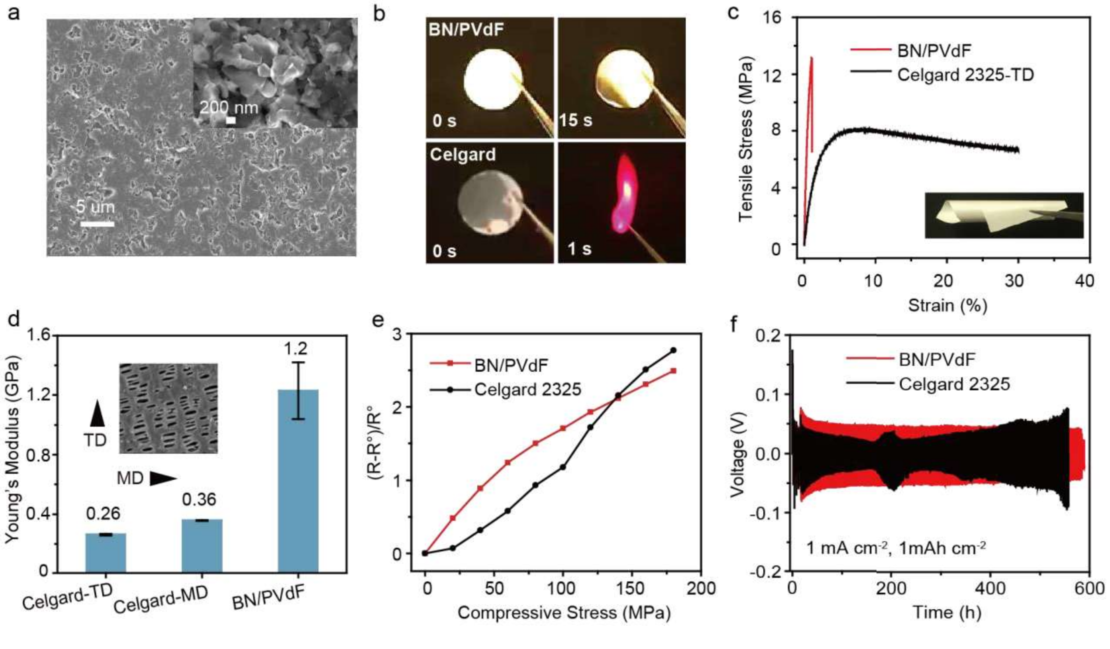

**Figure 4.** (a) An SEM image of the as-fabricated BN/PVdF separator with the inset showing the BN nanosheets after sonication. (b) Ignition tests of Celgard 2325 separator and BN/PVdF film wetted by liquid electrolyte (1M LiTFSI in DOL/DME (v/v, 1:1)). (c) The strain-stress curves of PE separator (Celgard 2325 at transverse direction) and BN/PVdF film with the inset showing the flexible BN/PVdF film. (d) The Young's modulus of a BN/PVdF separator and a PE separator along its machinery direction (MD) and transverse direction (TD). (e) The dependence of resistance upon compressive stress of stainless steel (SS)/separator/SS cells, where the separator layer is BN/PVdF (red) or commercial separator (black). (f) The voltage profile of Li/Li symmetric cells at 1.0 mA cm$^{-2}$ with different separators, BN/PVdF (red) and commercial separator (black).

After optimizing each component, the electrodes and separator are integrated into a structural Li-S battery. The battery displays an initial capacity of 1266 mAh g$^{-1}$(sulfur) when the weight ratio of the electrolyte to sulfur is 20. After a slight drop to 1101 mAh g$^{-1}$ at the 10th cycle, the capacity stabilizes at 1030 mAh g$^{-1}$ after 200 cycles (Fig. 5a). This performance exceeds that of conventional Li-S batteries with particle-based electrodes. Rate performance test shows the discharge capacity reaching 1228, 1069, 923 and 791 mAh g$^{-1}$ at 0.1, 0.2, 0.5 and 1 C rate respectively, much higher than regular cells, which typically displays discharge capacities of 692, 477, 268 and 60 mAh g$^{-1}$ at the same rates above (Fig. 5b). The higher discharge capacity along with smaller polarization confirms the superiority of electrodes with carbon fiber-based strcutural skeletons. Based on the good electrochemical performance, an energy density of 51 Wh kg$^{-1}$ (based on the weight of 1 M polysulfide catholyte, 2X lithium and OCF) is estimated, which exceeds that of the previous reports on structural batteries or supercapacitors (Fig. 5c)[4, 8, 15, 16, 30, 31]. With further increase polysulfide concentration (*e.g.* 5 M [S]), the energy density is expected to increase to 127 Wh kg$^{-1}$ with CF-based electrode and electrolyte considered.

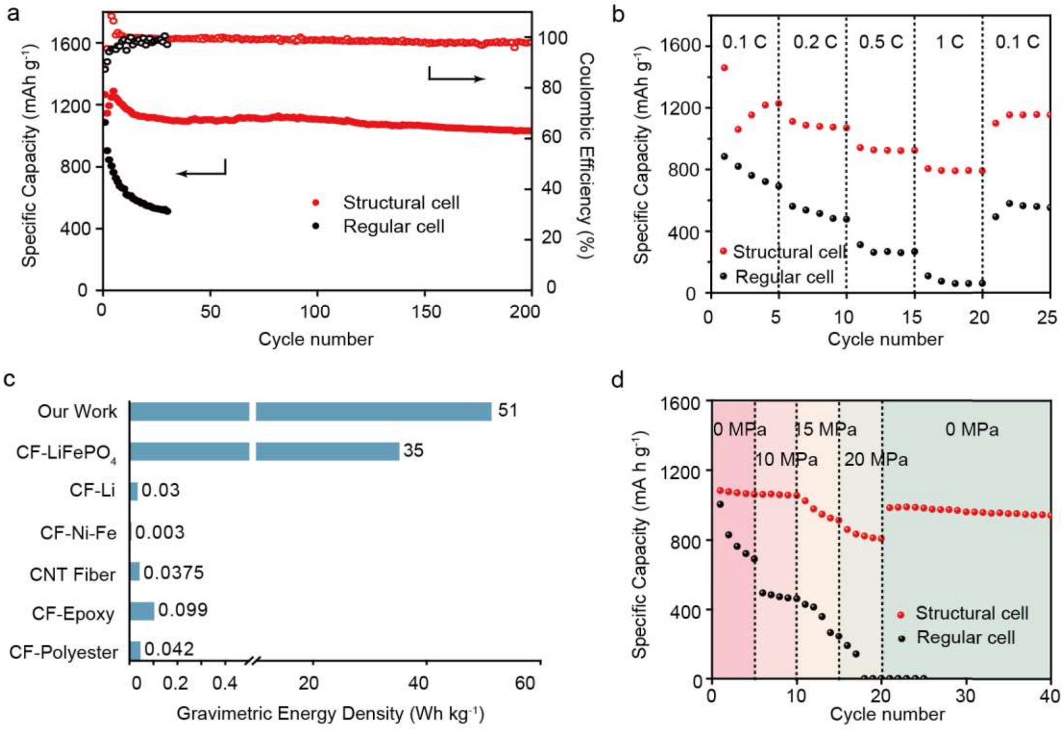

**Figure 5.** The comparison of cycling performance of the optimized structural battery and the conventional particle electrode-based battery at (a) 0.2 C and (b) different C-rates. (c) Summary of the calculated energy densities of the various structural batteries and supercapacitors. (d) The electrochemical performance of a

structural Li-S cell and a regular Li-S cell at various compressive stresses. The structural battery system consists of the optimized Li/OCF 400 °C 15 min, BN/PVdF separator, lithium polysulfide on OCF 500 °C 2 h, while the regular cell uses lithium foil, celgard 2325 separator and particle-based cathode with the same sulfur loading of 1.0 mg $cm^{-2}$.

Besides testing in ambient conditions, we also investigate the cells at different compressive stresses (up to 20 MPa). As shown in Fig. 5d, the structural cell exhibits a discharge capacity of 1093 mAh $g^{-1}$ when a compressive stress of 10 MPa is applied, much higher than 429 mAh $g^{-1}$ of the regular cell. Even when the stress increases to 20 MPa, it still remains at 981 mAh $g^{-1}$ for the structural cell. In contrast, the capacity of the regular Li-S cell decays to almost zero, suggesting failure of the battery. This result demonstrates that the structural cell possesses excellent resistance to mechanical stress. After the stress is removed, the capacity in structural cell is recovered to 983 mAh $g^{-1}$ and the BN/PVdF film survives intact. In contrast, the conventional Li-S cell shows no capacity left, and its voltage profile indicate that the cell's internal resistance remarkably increases, which is likely to arise from cracks of electrode and the closure of pores in separator under high pressure.

### 1.3 Summary

In summary, we proposed a feasible strategy to build a multifunctional structural energy storage platform so as to enhance the mechanical strength of structural batteries. This can be realized by utilizing electrodeposition-like reactions to coat active materials conformably onto a mechanically strong conductive skeleton, thereby avoiding the delamination that conventional particle-based electrodes encountered. The effectiveness of this strategy is demonstrated using an OCF-enhanced Li-S battery. The mechanical strength and modulus of the reinforced lithium anode and sulfur cathode are 10-20 times better than their conventional counterparts. A novel BN/PVdF separator is also developed with good mechanical robustness and thermal stability. This cell shows an attractive electrochemical performance. The initial capacity reaches 1266 mAh $g^{-1}$ and remains at 1030 mAh $g^{-1}$ after 200 cycles. Our design provides a potential for structural Li-S battery, which can be further applied to other systems, such as metal-air batteries and Li-$I_2$ batteries.

## 2. Solid-state batteries with nacre-like solid electrolyte

Solid state batteries are attractive for structural energy storage since it is much safer than current Li-ion batteries with flammable liquid electrolyte. However, ceramic solid electrolyte is highly fragile so that it is easy to break. On the other side, using polymer electrolyte will greatly reduce mechanical strength of the electrolyte. Here we developed a new structure of solid electrolyte inspired by nacre, called nacre-like electrolyte. In nacre, ceramic microplates are aligned but separated by polymer. The high interfacial strength between ceramic and polymer provides both high mechanical modulus and excellent fracture resilience.

In our design, $Li_{1.5}Al_{0.5}Ge_{1.5}(PO_4)_3$ (LAGP) solid electrolyte microplates with thickness of ~10-20 μm and size of 50-100 μm are separated by polymer electrolyte. Hence it is both tough and strong. The ionic conductivity reaches $10^{-3}$ S $cm^{-1}$ at room temperature. Such composite electrolyte is combined with a $LiFePO_4$ cathode and a lithium metal anode for full cell test. While such a cell with nacre-like electrolyte can provide steady cycling under a force of 10 N for over 100 cycles, a cell with the same configuration but pure ceramic electrolyte fails immediately after the same force is applied. This demonstrates that the nacre-like electrolyte is stronger against flexing deformation.

Such nacre-like ceramic/polymer electrolyte (NCPE) is fabricated by the procedure in Fig. 6b. A liquid suspension of ceramic electrolyte particles and polymer additives were coated onto a Mylar substrate (Step 1), and ceramic films after solvent evaporation were stacked and laminated together (Step 2). The freestanding films were then sintered at 850 °C to form a multi-layered ceramic stack (Step 3), and subsequently soaked in polymer electrolyte dissolved in a solvent under vacuum. As a result, the polymer electrolyte is able to infiltrate the multi-layer stack and stick to the ceramic surface (Step 4). The composite was then hot pressed at 80°C to break the ceramic electrolyte films into platelets and enable the polymer electrolyte to fill all gaps simultaneously, forming the nacre structure and further improving the contact between polymer and ceramic platelets (Step 5). The as-fabricated composite solid-state electrolyte was then assembled with lithium metal anode and $LiFePO_4$ cathode in a pouch cell configuration (Step 6). Such NCPEs-based cell can serve as a promising dual-functional component for both energy storage units and load-bearing elements in various devices, such as vehicles and aircraft. Three different polymer electrolytes, PEO, PEA, and epoxy, were demonstrated for fabricating NCPEs. PEO is chosen as it is a low-cost, widely used polymer electrolytes.[32, 33] PEA electrolyte is chosen to enable cycling at room temperature,[34] and epoxy electrolyte[35, 36] is to further demonstrate versatility of the proposed process.

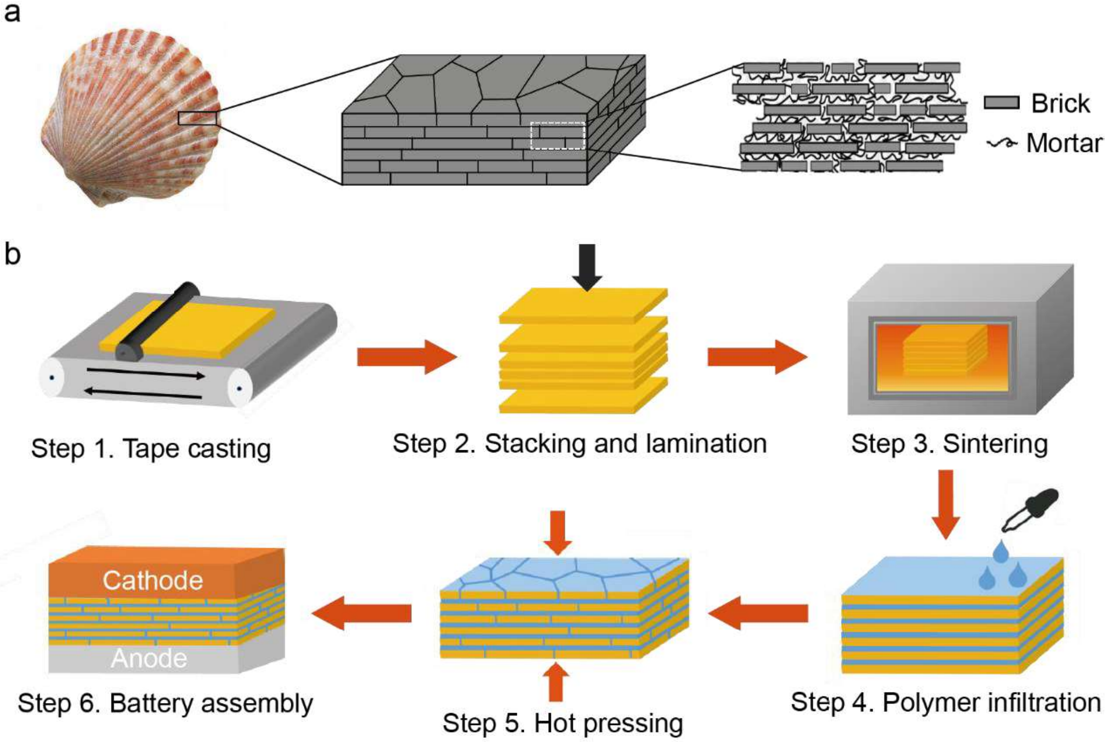

**Figure 6.** The design and fabrication of nacre-like ceramic/polymer composite electrolyte. (a) Schematic of staggered "brick-and-mortar" microstructure in nacre. (b) Schematic of the bottom-up fabrication process of NCPEs and battery assembly.

5 cm × 5 cm NCPEs are prepared, with LAGP-PEO serving as an example (Fig. 7a), wherein the translucent nature indicates large grain size and dense film since otherwise grain boundaries and pores will cause significant light scattering, rendering the film opaque. Thermal gravimetric analysis (TGA) indicates that the weight percentage of LAGP "brick" are 96.5%, 95.1%, and 94.4% for LAGP-PEO, LAGP-PEA, and LAGP-Epoxy NCPEs, respectively, corresponding to the volume portion of 90.8%, 87.0%, and 85.9%, respectively (Fig. 7b). Scanning electron microscopic (SEM) images further confirm that ceramic micro-tablets are well aligned and closely packed, with the polymer electrolyte present between layers and inside gaps (Fig. 7c and Fig. 7d). The thickness and aspect ratio of as-fabricated individual LAGP tablets are ~15 μm and 10-15, respectively, and the total thickness of the composite electrolyte is 100-200 μm. Such a large aspect ratio is critical to enhancing the mechanical strength and toughness of the nacre-like electrolyte [37,

[38]. The thickness of the cohesive PEO layer is ~1 μm, which provides a soft but tough bridge between the brittle ceramic layers. Similar morphology and structure are also observed in LAGP-PEA and LAGP-Epoxy NCPEs. In the future, we expect that the thickness of individual tablet and entire electrolyte can be reduced to ~ 3-5 μm and ~ 10-20 μm after optimization, which is attractive for practical cells.

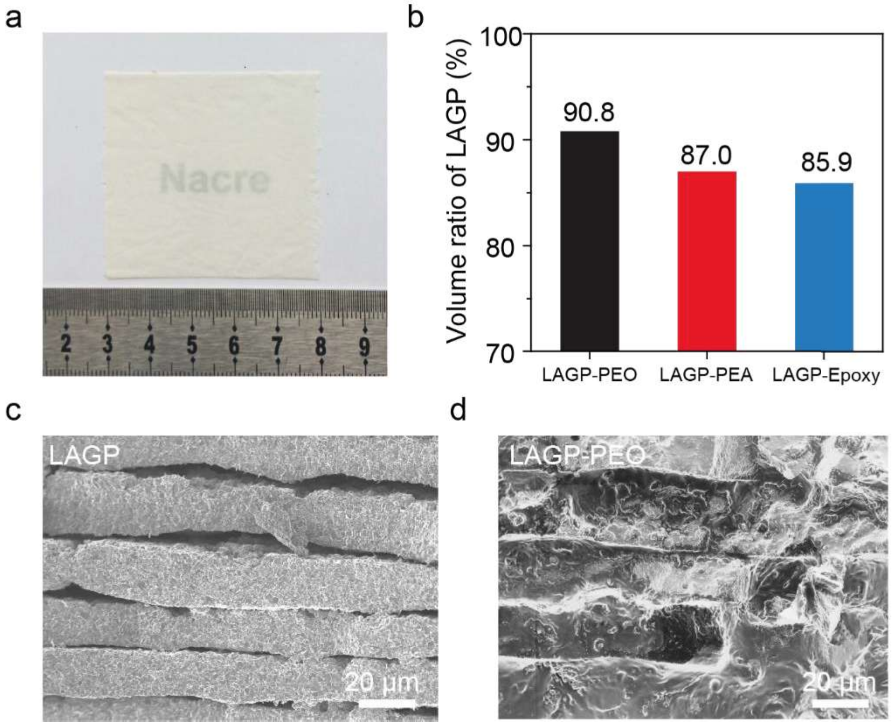

**Figure 7.** Characterizations of NCPEs. (a) An optical image of as-fabricated LAGP-PEO NCPEs with a size of 5 cm × 5 cm. (b) The volumetric percentage of LAGP ceramic in various NCPEs of LAGP-PEO, LAGP-PEA, and LAGP-Epoxy. (c and d) Cross-sectional SEM images of (c) layered LAGP tablets before PEO infiltration and hot pressing and (d) an LAGP-PEO NCPE film showing the staggered microstructure after hot pressing.

The as-fabricated NCPEs show significantly improved mechanical properties compared to pure ceramic and pure polymer electrolytes, as validated by ball impact, three-point bending and indentation tests. All results show that NCPEs are much tougher than pure LAGP ceramic electrolyte, and have a much higher modulus than polymer electrolytes. First, in ball impact tests, a stainless steel ball with a weight of 8.4 g is dropped from various heights onto the solid electrolyte. The pure LAGP film breaks into pieces when the ball is dropped from a height of 20 cm, while the LAGP-PEO film maintains its integrity even when the ball is dropped from 40 cm (Fig. 8a). This visual representation means the designed nacre-like composite electrolyte is much tougher than the pure ceramic film.

Besides qualitative ball dropping tests, the stiffness and strength of the LAGP-PEO NCPE film are quantitatively determined by three-point flexural tests. The LAGP-PEO film has a high ultimate flexural strength of 30.2 MPa, slightly lower than that of pure LAGP film (34.3 MPa, Fig. 8b), but are ~30 times higher than the PEO polymer (~ 1 MPa). Furthermore, the failure strain for LAGP-PEO is roughly 1.1%, about one order of magnitude higher than that of pure LAGP film (0.13%). This is consistent with the layer-by-layer fracture behavior but not straight crack shown in previous work [39, 40], which also shows the nonlinear and step-like behavior. Compared to pure LAGP with a flexural modulus of 25.6 GPa, the LAGP-PEO, LAGP-PEA and LAGP-Epoxy NCPEs film are more flexible with lower flexural modulus of 7.8, 7.2 and 4.5 GPa, respectively (Fig. 8c), but these values are significantly higher than that of pure polymer electrolyte and composite electrolytes (96 MPa in reference [41] and 850 MPa in reference [42]). Such enhanced mechanical strength and fracture strain originate from the synergic interaction of hard ceramic tablets and tough polymer interfacial layers arranged in the "brick-and-mortar" microstructure. In the future, with optimized annealing process to further enhance the mechanical strength of LAGP ceramic itself (e.g. to ~ 100 MPa in common ceramics), the mechanical properties of NCPEs are expected to be further enhanced.

Additionally, other NCPE systems of LAGP-PEA and LAGP-Epoxy NCEs exhibit similar enhancements in both mechanical strength and failure strain. When compared to their corresponding polymers, the ultimate flexural strengths increase from 0.06 MPa to 20.4 MPa for LAGP-PEA, and from 1.5 MPa to 25.6 MPa for LAGP-Epoxy. In the future, the mechanical properties can be further optimized by controlling the thickness of ceramic films and adjusting the pressure in the hot press.

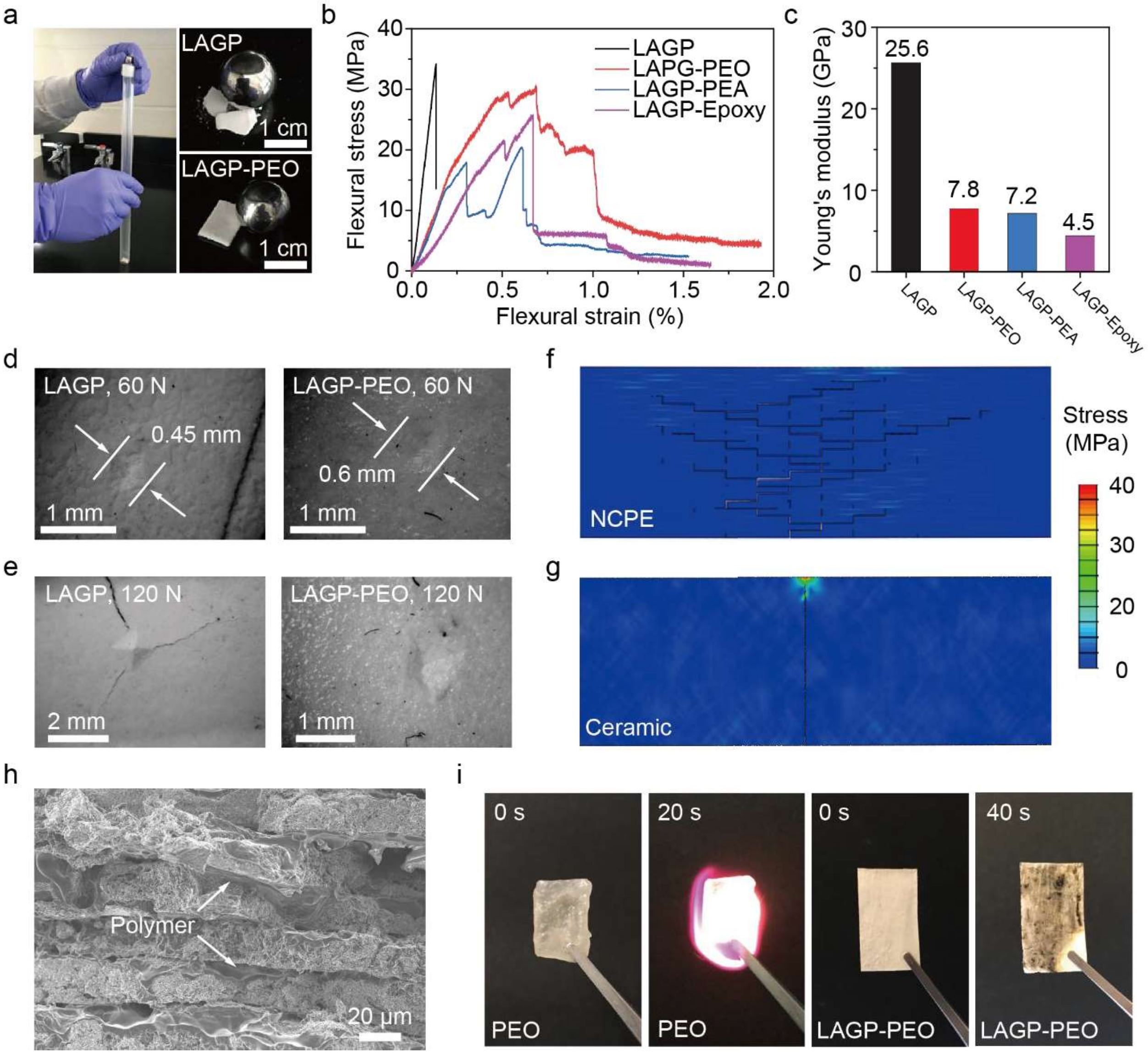

**Figure 8.** Mechanical properties of NCPEs and toughening mechanisms. (a) Impact test of as-fabricated LAGP-PEO NCPE and pure ceramic films, showing higher impact resistance in a LAGP-PEO NCPE film. The ball dropped from 20 cm for pure LAGP ceramic and from 40 cm height for NCPE, respectively. (b) Flexural stress-strain curves of NCPEs and pure ceramic films through three-point bending tests. (c)

Young's modulus of NCPEs and pure ceramic. Vickers indentation of pure ceramic film and LAGP-PEO NCPE film using loads of (d) 60 N and (e) 120 N. (f and g) Nonlinear finite element simulations of (f) Tortuous crack propagation through interfacial polymer failure in an NCPE film and (g) straight crack in a pure ceramic film under the same force load. (h) Fractured surface of LAGP-PEO NCPE showing extensive interfacial failure. (i) Optical images of ignition tests on pure PEO and LAGP-PEO NCPE films.

Vickers indentation tests were further conducted to evaluate sample hardness and toughness. LAGP-PEO NCPE is selected as an example. Given that $HV = 0.1891F\ d^{-2}$, where $HV$ is the hardness number, $F$ is the applied load and $d$ is the diagonal left by the indenter, we find that the hardness for pure ceramic film (~ 50 MPa) is higher than that for LAGP-PEO NCPE film (~31 MPa) under the same load of $F$ = 60 N (Fig. 8d). This agrees with results from three-bending tests in Fig. 8b. However, under a load of $F$ = 120 N, a long and straight crack of $L$ = 5 mm is observed in pure LAGP film, while negligible crack initiation (< 0.1 mm) but only a larger plastic indent is left in the NCPE film (Fig. 8e). According to the well-known Evans-Charles formula for evaluating fracture toughness, $\mathrm{K}_{IC} \propto 0.16 \left(\frac{\mathrm{HV}}{\mathrm{E}}\right)^{-0.5} F\ L^{-1.5}$ ($E$ is the modulus), the LAGP-PEO NCPE can accommodate more strain energy than pure ceramic [43].

To determine mechanisms responsible for the improvement in toughness for nacre-like composite electrolytes, numerical simulation was carried out on crack propagation inside NCPEs with regular "brick-and-mortar" arrangement subjected to three-point bending. Fig. 8f and Fig. 8g show the stress distribution and crack propagation when a ceramic/polymer nacre-like film and a pure ceramic film with the same dimension undergo a fixed deflection of 1 mm, respectively. This displacement load corresponds to a flexural strain of 1.8% and can thus cause catastrophic failure in the pure ceramic film as a result of the straight crack since 1.8% is well beyond failure strain in ceramics (~ 0.13%). For the nacre-like composite structure, however, the maximum stress in ceramic layers is only 10 MPa, much less than the failure strength of ceramic. The stress release mechanism is the failure of interfacial polymer and the crack deflection at polymer interfaces with a torturous path, which does not propagate in the ceramic layer. The failed interfaces are subsequently dominated by interfacial sliding and plastic deformation, which toughens the composite and resists its catastrophic failure [38, 44]. The SEM image of NCPEs' fractured surface (Fig. 8h) illustrates extensive interfacial delamination between LAGP ceramic tablets and densely adhered polymer bridging, which confirms the efficient energy dissipation at interfaces. Both simulation and experimental evidence clearly show that NCPEs have advantages regarding flexibility and fracture toughness.

Furthermore, the LAGP-PEO NCPE film has high thermal stability and it does not ignite over the fire, as shown in Fig. 8i and the Supporting Video. In contrast, pure PEO electrolyte can be ignited when exposed to a flame. This significant contrast further demonstrates the enhanced safety of NCPEs for battery applications. Through comparison of mechanical properties, the LAGP-polymer NCPEs outperforms to other state-of-the-art SSEs regarding ultimate flexural strength and fracture strain [45-52], underpinning promising applications of the NCPE for safe, impact-resistant and load-bearing batteries.

In addition to excellent mechanical properties, NCPEs also exhibit high ionic conductivity. With the nacre-like microstructure, the conductivity of LAGP-PEO NCPE reaches $1.25 \times 10^{-4}$ S cm$^{-1}$ at 25 ºC and $1.3 \times 10^{-3}$ S cm$^{-1}$ at 60 ºC in electrochemical impedance spectroscopy (EIS) tests. This is much higher than the polymer phase itself ($1.0 \times 10^{-5}$ S cm$^{-1}$ at 25 ºC) and is close to that of pure LAGP pellet ($2.0 \times 10^{-4}$ S cm$^{-1}$ at 25 ºC). The value is also consistent with a simple parallel model of ceramic and polymer electrolytes based on their volume portion, indicating low interfacial impedance. The conductivity of LAGP-PEO NCPE is also stable over 400 h. The LAGP-PEA and LAGP-Epoxy also exhibit ionic conductivities over $7.4 \times 10^{-4}$ and $8.4 \times 10^{-4}$ S cm$^{-1}$ at room temperature, respectively, which are close to the ionic conductivity of conventional liquid electrolytes with separator presented. The high conductivities of NCPEs are attributed to the high volume portion of the conductive ceramic electrolyte and the small thickness of the interfacial polymer layer.

To demonstrate enhanced stability of NCPEs under mechanical load, electrochemical cycling of NCPE-based cells under mechanical deformation is further carried out. First, pouch cells with the same electrolyte size of 5.3 cm × 2.3 cm × 0.5 mm but different electrolyte compositions (pure LAGP, pure PEA, and LAGP–PEA NCPE) are subjected to three-point bending tests (Fig. 9a–d). When a force of 6 N is applied, the LFP/Li full cell with pure LAGP ceramic electrolyte breaks immediately with a small displacement of 0.1 mm (Fig. 9b), as a result of the brittleness of ceramic. Moreover, the cell with pure PEA gel electrolyte shows a large deformation of 5.6 mm due to the softness of gel electrolytes (Fig. 9c). In contrast, the cell with LAGP–PEA NCPE only exhibits a small deformation of 0.6 mm, 10% of that with gel electrolyte (Fig. 5d). This indicates that the NCPE is much stiffer than the PEA electrolyte. Moreover, the NCPE does not break under such load, suggesting that it can absorb more energy than pure ceramic during deformation.

The enhanced mechanical properties of NCPEs are further validated by battery operation under mechanical deformation. Cells with electrolyte dimension of 53 × 53 × 0.5 $mm^3$ are subjected to the same point load of 10 N, corresponding to a high-stress level of 15 MPa in the NCPE electrolyte based on the flexural displacement. All electrode sizes are 5 cm × 5 cm with a capacity of 14 mAh, and the lithium thickness is 40 µm. Thin layers of PEA electrolyte are coated on the LFP cathode and Li anode for reducing interfacial resistance in all cells.

These cells with NCPE, LAGP, and PEA electrolytes are all cycled at 0.2 C for 20 cycles first, which show similar capacity and cycling performance (Fig. 9e). However, once 10 N is applied, the capacity of the LAGP cell quickly drops to nearly zero after 3 cycles (Fig. 9e), and the capacity of the PEA cell shows a sudden drop to 93.7 mAh $g^{-1}$, followed by a quick decay to 60.2 mAh $g^{-1}$ after 100 cycles (Fig. 9e). These results indicate that neither soft PEO nor brittle LAGP electrolyte can withstand external force. On the other side, the NCPE cell shows no apparent capacity loss after the load is applied, and the capacity retention is as high as 95.6% after 100 cycles. Stable CE of 99.9% and smooth voltage profiles are also achieved (Fig. 9e). As a further demonstration, the NCPE cell can still power multiple LEDs after a point load of 10 N is applied (Fig. 9f and Fig. 9g). Such significantly enhanced mechanical properties of NCPE ensure better stability in solid-state batteries against external impact. Results above also suggest that the nacre-like design is attractive for structural energy storage, where batteries are used to replace structural components in vehicles and aircraft for weight reduction but need to withstand high mechanical loads [53, 54].

In summary, we have fabricated nacre-like ceramic/polymer composite electrolytes with the "brick-and-mortar" microstructure, demonstrating both high ultimate flexural strength and high toughness, and resolving the dilemma between high strength/low toughness in pure ceramic electrolytes and low strength/high toughness in pure polymer electrolytes. The mechanically robust NCPEs allow high capacity retention of 95.6% over 100 cycles in an LFP/Li pouch cell, even when it is subjected to an external point load. In contrast, cells based on pure ceramic and pure polymer electrolytes show sudden capacity drop and quick fading when the same magnitude of the mechanical load is applied. Therefore, the proposed nacre-like configuration presents a promising load-bearing ceramic/polymer composite electrolyte for solid-state batteries and even structural energy storage with high energy density, excellent mechanical properties, and high thermal stability. Among the three nacre-like electrolytes above, LAGP-PEO has the highest mechanical strength and modulus while LAGP-PEA has better cycling performance than the epoxy system. As PEO nacre does not work well at RT, we consider LAGP-PEA has a balanced and most attractive performance among these three systems.

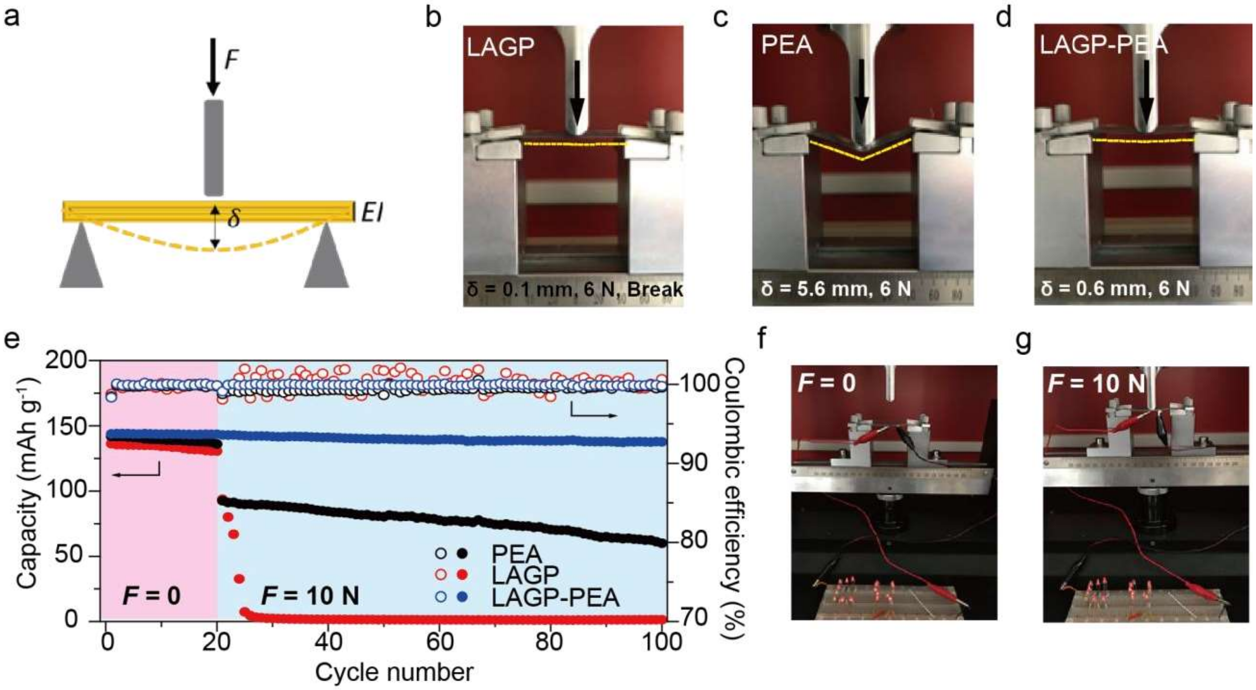

**Figure 9.** Mechanical stability of NCPEs-based full cells. (a) Schematic of indenting a suspended pouch cell under point force. (b-d) Pouch cells with (b) pure LAGP under 0.1 mm displacement (c) LAGP-PEA NCPE under 0.6 mm displacement and 6 N load, and (d) pure PEA film under 6 N load. (e) The cycling performance of LFP/PEA/Li, LFP/LAGP/Li and LFP/LAGP-PEA NCPE/Li cells at 0.2 C under point load of 10 N. (f and g) A structural LFP/LAGP-PEA NCPE/Li pouch cell lighting a series of LEDs under (f) no load and (g) 10 N load. 40 μm-thin lithium was used in all these pouch cells.

Publication list

AFOSR grant has a major contribution:

1. Huang, W. L.; Wang, P. Y.; Chitu, A.; Jin, T. W.; Yang, Y.* Mechanically-robust structural lithium-sulfur battery with high energy density, submitted to *Energy Storage Materials*.

2. Li, A.; Liao, X.; Zhang, H.; Shi, L.; Wang, P.; Cheng, Q.; Borovilas, J.; Li, Z.; Huang, W.; Fu, Z.; Dontigny, M.; Zaghib, K.; Meyers, K.; Chuan, X.; Chen, X.*; Yang, Y.*; Nacre-inspired Composite Electrolytes for Load-bearing Solid-state Lithium Metal Batteries. *Advanced Materials*. 32(2), 1905517 (2020).

AFOSR grant has a minor contribution:

1. Lu, C.; Yang, Y.; Chen X.*; Ultrathin conductive graphitic carbon nitride assembly through van der Waals epitaxy toward high energy-density flexible supercapacitors, *Nano Letters*, 19(6), 4103-4111 (2019).

2. Mandal, J.; Jia, M.; Overvig, A.; Fu, Y.; Che, E.; Yu, N.; Yang, Y.*; Porous Polymers with Switchable Optical Transmittance for Optical and Thermal Regulation. *Joule*, 3(12), 3088-3099 (2019).

3. Zhai, H.; Gong, T.; Xu, B.; Cheng, Q.; Paley, D.; Qie, B.; Jin, T.; Fu, Z.; Tan, L.; Lin, Y.-H.; Nan, C.-W.; Yang, Y.*; Stabilizing Polyether Electrolyte with a 4 V Metal Oxide Cathode by Nanoscale Interfacial Coating. *ACS Applied Materials & Interfaces*, 11(32), 28774-28780 (2019).

4. Song, Q.; Li, A.; Shi, L.; Cheng, Q.; Feric, T. G.; Fu, Y.; Zhang, H.; Li, Z.; Wang, P.; Li, Z.; Zhai, H.; Wang, X.; Dontigny, M.; Zaghib, K.; Park, A.-H.; Myers, K.; Chuan, X.; Yang, Y.*; Thermally stable, nano-porous and eco-friendly sodium alginate/attapulgite separator for lithium-ion batteries. *Energy Storage Materials*, 22, 48-56(2019).

5. Jin, T.; Wang, Y.; Hui, Z.; Qie, B.; Li, A.; Paley, D.; Xu, B.; Wang, X.; Chitu, A.; Zhai, H.; Gong, T.; Yang, Y.*; Nonflammable, Low-Cost, and Fluorine-Free Solvent for Liquid Electrolyte of Rechargeable Lithium Metal Batteries. *ACS Applied Materials & Interfaces*, 11(19), 17333-17340 (2019).

6. Cheng, Q.; Li, A.; Li, N.; Yan, K.; Li, S.; Amirali Z.; Li, T.; Huang, W.; Li, A.; Jin, T.; Song, Q.; Xu, W.; Ni, N.; Zhai, H.; Martin D.; Karim Z.; Xiuyun C.; Su, D.; & Yang Y.*; Stablizing Solid Electrolyte-Anode Interface in Li-Metal Batteries by Boron Nitride-Based Nanocomposite Coating. *Joule*, 3(6), 1510-1522 (2019).

7. Wang, X.; Zhai, H.; Qie, B.; Cheng, Q.; Li, A.; Borovilas, J.; Xu, B.; Shi, C.; Jin, T.; Liao, X.; Li, Y.; He, X.; Du, S.; Fu, Y.; Dontigny, M.; Zaghib, K.; & Yang, Y.*; Rechargeable solid-state lithium metal batteries with vertically aligned ceramic nanoparticle/polymer composite electrolyte. *Nano Energy*, 60, 205-212 (2019).

8. Cheng, Q.; Xu, W.; Qin, S.; Das, S.; Jin, T.; Li, A.; Li, A. C.; Qie, B.; Yao, P.; Zhai, H.; Shi, C.; Yong, X.; Yang, Y.*; Full Dissolution of Li2S8 to Li2S in Safe Eutectic Solvent for Rechargeable Lithium-Sulfur Batteries. *Angewandte Chemie, International Edition*, 58, 1-6 (2019).

9. Qian, G.; Liao, X.; Zhu, Y.; Pan, F.; Chen, X.; Yang, Y.*; Designing Flexible Lithium-Ion Batteries by Structural Engineering. *ACS Energy Letters*, 4, 3, 690-701 (2019).

10. Xu, B.; Zhai, H.; Liao, X.; Qie, B.; Mandal, J.; Gong, T.; Tan, L.; Yang, X.; Sun, K.; Cheng, Q.; Chen, M.; Miao, Y.; Wei, M.; Zhu, B.; Fu, Y.; Li, A.; Chen, X.; Min, W.; Nan, C.*; Lin, Y.*; Yang, Y.*; Porous Insulating Matrix for Lithium Metal Anode with Long Cycling Stability and High Power, *Energy Storage Materials* 17, 31-37 (2019).

11. Shi, C.; Wang, T.; Liao, X.; Qie, B.; Yang, P.; Chen, M.; Wang, X.; Srinivasan, A.; Cheng, Q.; Li, A.; Chen, X.; Yang, Y.*; Accordion-like Stretchable Li-ion Batteries with High Energy Density, *Energy Storage Materials*, 17, 136-142 (2019).

12. Liao, X.; Shi, C.; Wang, T.; Qie, B.; Chen, Y.; Yang, P.; Cheng, Q; Zhai, H.; Chen, M.; Wang, X.; Chen, X.*; Yang, Y.*; High-Energy-Density Foldable Battery Enabled by Zigzag-like Design, *Advanced Energy Materials*, 1802998 (2018).

13. Mandal, J.; Fu, Y.; Overvig, A.; Jia, M.; Sun, K.; Shi, N.; Zhou, H.; Xiao, X.; Yu, N.; Yang, Y.*; Hierarchically porous polymer coatings for highly efficient passive daytime radiative cooling. *Science*, 362(6412), 315-319 (2018).

References

1. Kim, H.C. & Wallington, T.J. Life-Cycle Energy and Greenhouse Gas Emission Benefits of Lightweighting in Automobiles: Review and Harmonization. *Environmental Science & Technology* **47**, 6089-6097 (2013).
2. Tenney, D.R., Starke Jr, E.A., Newman Jr, J.C., Heyman, J. & Bales, T.T. Structural Framework for Flight II: NASA's Role in Development of Advanced Composite Materials for Aircraft and Space Structures. (2019).
3. Flouda, P. et al. Interfacial Engineering of Reduced Graphene Oxide for Aramid Nanofiber-Enabled Structural Supercapacitors. *Batteries & Supercaps* **2**, 464-472 (2019).
4. Senokos, E. et al. Energy storage in structural composites by introducing CNT fiber/polymer electrolyte interleaves. *Scientific reports* **8**, 3407 (2018).
5. Silva-Leon, J., Cioncolini, A., Nabawy, M.R., Revell, A. & Kennaugh, A. Simultaneous wind and solar energy harvesting with inverted flags. *Applied Energy* **239**, 846-858 (2019).
6. Shanks, K. et al. A> 3000 suns high concentrator photovoltaic design based on multiple Fresnel lens primaries focusing to one central solar cell. *Solar Energy* **169**, 457-467 (2018).
7. Kwon, S.R. et al. Mechanically Strong Graphene/Aramid Nanofiber Composite Electrodes for Structural Energy and Power. *ACS Nano* **11**, 6682-6690 (2017).
8. Moyer, K. et al. Carbon fiber reinforced structural lithium-ion battery composite: Multifunctional power integration for CubeSats. *Energy Storage Materials* (2019).
9. on Tung, S., Fisher, S.L., Kotov, N.A. & Thompson, L.T. Nanoporous aramid nanofibre separators for nonaqueous redox flow batteries. *Nature communications* **9**, 4193 (2018).
10. Snyder, J.F., Carter, R.H. & Wetzel, E.D. Electrochemical and mechanical behavior in mechanically robust solid polymer electrolytes for use in multifunctional structural batteries. *Chemistry of Materials* **19**, 3793-3801 (2007).
11. Carlson, T., Ordeus, D., Wysocki, M. & Asp, L.E. Structural capacitor materials made from carbon fibre epoxy composites. *Composites Science and Technology* **70**, 1135-1140 (2010).
12. Asp, L.E. & Greenhalgh, E.S. Structural power composites. *Composites Science and Technology* **101**, 41-61 (2014).
13. Muralidharan, N. et al. Carbon Nanotube Reinforced Structural Composite Supercapacitor. *Sci Rep* **8**, 17662 (2018).
14. Flouda, P., Shah, S.A., Lagoudas, D.C., Green, M.J. & Lutkenhaus, J.L. Highly Multifunctional Dopamine-Functionalized Reduced Graphene Oxide Supercapacitors. *Matter* (2019).
15. Johannisson, W. et al. Multifunctional performance of a carbon fiber UD lamina electrode for structural batteries. *Composites Science and Technology* **168**, 81-87 (2018).
16. Meng, C. et al. Multifunctional Structural Ultrabattery Composite. *Nano Lett* **18**, 7761-7768 (2018).
17. Wong, E. et al. (ARMY RESEARCH LAB ABERDEEN PROVING GROUND MD, 2007).
18. Xu, R. et al. Cathode-Supported All-Solid-State Lithium–Sulfur Batteries with High Cell-Level Energy Density. *ACS Energy Letters* **4**, 1073-1079 (2019).
19. Li, H., Wang, S., Feng, M., Yang, J. & Zhang, B. Self-assembly and performances of wrinkled rGO@ carbon fiber with embedded SnO 2 nanoparticles as anode materials for structural lithium-ion battery. *Journal of materials science* **53**, 11607-11619 (2018).
20. Carlstedt, D., Marklund, E. & Asp, L.E. Effects of state of charge on elastic properties of 3D structural battery composites. *Composites Science And Technology* **169**, 26-33 (2019).
21. Chu, H. et al. Achieving three-dimensional lithium sulfide growth in lithium-sulfur batteries using high-donor-number anions. *Nature communications* **10**, 188 (2019).
22. Wang, Z. et al. Self-Supported and Flexible Sulfur Cathode Enabled via Synergistic Confinement for High-Energy-Density Lithium–Sulfur Batteries. *Advanced Materials* **31**, 1902228 (2019).

23. Lin, D.C. et al. Layered reduced graphene oxide with nanoscale interlayer gaps as a stable host for lithium metal anodes. *Nature Nanotechnology* **11**, 626-632 (2016).
24. Go, W. et al. Nanocrevasse-Rich Carbon Fibers for Stable Lithium and Sodium Metal Anodes. *Nano Lett* **19**, 1504-1511 (2019).
25. Kim, J.H. et al. Nanomat Li-S batteries based on all-fibrous cathode/separator assemblies and reinforced Li metal anodes: towards ultrahigh energy density and flexibility. *Energy & Environmental Science* **12**, 177-186 (2019).
26. Luo, W. et al. Protection of boron nitride nanosheets by atomic layer deposition toward thermal energy management applications. *Nano Energy* **40**, 149-154 (2017).
27. Luo, W. et al. A Thermally Conductive Separator for Stable Li Metal Anodes. *Nano Lett* **15**, 6149-6154 (2015).
28. Yao, P. et al. PVDF/Palygorskite nanowire composite electrolyte for 4 V rechargeable lithium batteries with high energy density. *Nano letters* **18**, 6113-6120 (2018).
29. Cheng, Q. et al. Stabilizing Solid Electrolyte-Anode Interface in Li-Metal Batteries by Boron Nitride-Based Nanocomposite Coating. *Joule* **3**, 1510-1522 (2019).
30. Wang, Y., Qiao, X., Zhang, C. & Zhou, X. Development of All-Solid-State Structural Supercapacitor Using an Epoxy Based Adhesive Polymer Electrolyte. *ECS Transactions* **72**, 31-44 (2016).
31. Deka, B.K., Hazarika, A., Kim, J., Park, Y.-B. & Park, H.W. Multifunctional CuO nanowire embodied structural supercapacitor based on woven carbon fiber/ionic liquid–polyester resin. *Composites Part A: Applied Science and Manufacturing* **87**, 256-262 (2016).
32. Manthiram, A., Yu, X. & Wang, S. Lithium battery chemistries enabled by solid-state electrolytes. *Nature Reviews Materials* **2**, 16103 (2017).
33. Zhai, H. et al. A Flexible Solid Composite Electrolyte with Vertically Aligned and Connected Ion-Conducting Nanoparticles for Lithium Batteries. *Nano Letters* **17**, 3182-3187 (2017).
34. Zeng, X.-X. et al. Reshaping Lithium Plating/Stripping Behavior via Bifunctional Polymer Electrolyte for Room-Temperature Solid Li Metal Batteries. *Journal of the American Chemical Society* **138**, 15825-15828 (2016).
35. Choi, C.S. et al. Synthesis and Properties of a Photopatternable Lithium-Ion Conducting Solid Electrolyte. *Advanced Materials* **30** (2018).
36. Hur, J.I., Smith, L.C. & Dunn, B. High Areal Energy Density 3D Lithium-Ion Microbatteries. *Joule* **2**, 1187-1201 (2018).
37. Barthelat, F. Designing nacre-like materials for simultaneous stiffness, strength and toughness: Optimum materials, composition, microstructure and size. *Journal of the Mechanics and Physics of Solids* **73**, 22-37 (2014).
38. Ni, Y., Song, Z., Jiang, H., Yu, S.-H. & He, L. Optimization design of strong and tough nacreous nanocomposites through tuning characteristic lengths. *Journal of the Mechanics and Physics of Solids* **81**, 41-57 (2015).
39. Zekoll, S. et al. Hybrid electrolytes with 3D bicontinuous ordered ceramic and polymer microchannels for all-solid-state batteries. *Energy & Environmental Science* **11**, 185-201 (2018).
40. Morits, M. et al. Toughness and Fracture Properties in Nacre‐Mimetic Clay/Polymer Nanocomposites. *Advanced Functional Materials* **27**, 1605378 (2017).
41. Yao, P. et al. PVDF/Palygorskite nanowire composite electrolyte for 4 V rechargeable lithium batteries with high energy density. *Nano letters* **18**, 6113-6120 (2018).
42. Wan, J. et al. Ultrathin, flexible, solid polymer composite electrolyte enabled with aligned nanoporous host for lithium batteries. *Nature nanotechnology*, 1 (2019).
43. Feng, Y., Zhang, T. & Yang, R. A Work Approach to Determine Vickers Indentation Fracture Toughness. *Journal of the American Ceramic Society* **94**, 332-335 (2011).
44. Gao, H.L. et al. Mass production of bulk artificial nacre with excellent mechanical properties. *Nat*

*Commun* **8**, 287 (2017).

45. Lin, D. et al. A Silica-Aerogel-Reinforced Composite Polymer Electrolyte with High Ionic Conductivity and High Modulus. *Adv Mater* **30**, e1802661 (2018).
46. Kim, S.-H. et al. Flexible/shape-versatile, bipolar all-solid-state lithium-ion batteries prepared by multistage printing. *Energy & Environmental Science* **11**, 321-330 (2018).
47. Zekoll, S. et al. Hybrid electrolytes with 3D bicontinuous ordered ceramic and polymer microchannels for all-solid-state batteries. *Energy & Environmental Science* **11**, 185-201 (2018).
48. Chen, L. et al. PEO/garnet composite electrolytes for solid-state lithium batteries: From "ceramic-in-polymer" to "polymer-in-ceramic". *Nano Energy* **46**, 176-184 (2018).
49. Yao, P. et al. PVDF/Palygorskite Nanowire Composite Electrolyte for 4 V Rechargeable Lithium Batteries with High Energy Density. *Nano Lett* **18**, 6113-6120 (2018).
50. Lin, D. et al. High Ionic Conductivity of Composite Solid Polymer Electrolyte via In Situ Synthesis of Monodispersed SiO2 Nanospheres in Poly(ethylene oxide). *Nano Letters* **16**, 459-465 (2016).
51. Liu, W. et al. Enhancing ionic conductivity in composite polymer electrolytes with well-aligned ceramic nanowires. *Nature Energy* **2**, 17035 (2017).
52. Fu, K.K. et al. Flexible, solid-state, ion-conducting membrane with 3D garnet nanofiber networks for lithium batteries. *Proc Natl Acad Sci U S A* **113**, 7094-7099 (2016).
53. Qian, G. et al. Designing flexible lithium-ion batteries by structural engineering. *ACS Energy Letters* **4**, 690-701 (2019).
54. Ladpli, P., Nardari, R., Kopsaftopoulos, F., Wang, Y. & Chang, F.-K. in European Workshop on Structural Health Monitoring (2016).